Journal of Power Sources 240 (2013) 114–121

Contents lists available at SciVerse ScienceDirect

Journal of Power Sources

journal homepage: www.elsevier.com/locate/jpowsour

Carbon corrosion fingerprint development and de-convolution of performance loss according to degradation mechanism in PEM fuel cells

S.R. Dhanushkodi [a], M. Tam [b], S. Kundu [b], M.W. Fowler [a,*], M.D. Pritzker [a]

[a] Department of Chemical Engineering, University of Waterloo, 200 University Ave. W, Waterloo, Ontario, Canada N2G 3G1
[b] Automotive Fuel Cell Cooperation Corp., 9000 Glenlyon Parkway, Burnaby, British Columbia, Canada V5J 5J8

HIGHLIGHTS

- Development of fingerprints of carbon loss for PEMFC.
- Development of a deconvolution method to estimate the performance losses due to Pt dissolution and carbon corrosion.
- Validation of Pt dissolution fingerprint method with experimental data.
- The limitations of the proposed method with different MEA types.

ARTICLE INFO

Article history:
Received 25 October 2012
Received in revised form
6 March 2013
Accepted 10 March 2013
Available online 28 March 2013

Keywords:
Carbon corrosion
Accelerated stress testing
Carbon fingerprint
Mixed degradation cycle
Deconvolution method and voltage loss breakdown

ABSTRACT

Carbon corrosion and Pt dissolution are the two major catalyst layer degradation modes in polymer electrolyte membrane fuel cells (PEMFC). One of the challenges in employing accelerated stress tests (ASTs) in PEMFCs is to relate the performance loss under a given set of conditions to a specific life-limiting factor. No well-established method is available to de-convolute the contributions to performance loss arising from carbon corrosion and Pt dissolution. In this study, a method to overcome this deficiency is demonstrated for three membrane electrode assemblies (MEAs) with different cathode Pt loading levels between 0.25 and 0.5 mg cm^{-2} and structures through the use of various ASTs favoring carbon corrosion, Pt dissolution or mixed carbon corrosion–Pt dissolution modes. A diagnostic indicator or 'fingerprint' for the performance loss due to carbon corrosion in the cathode layer (CCL) is first obtained for each MEA. This fingerprint is then applied to the performance loss measured during the mixed mode AST to deconvolute the contribution from Pt dissolution. Finally, this estimate of the contribution from Pt dissolution is compared to the performance loss measured directly during the AST in which Pt dissolution is dominant. The effectiveness of this approach is examined and its limitations are discussed.

1. Introduction

Polymer electrolyte membrane fuel cells (PEMFC) are attractive for automotive applications because of their high efficiency and low operating temperature that results in fast start-up time and low emissions [1]. However, the automotive sector requires highly stable fuel cell materials that can withstand a wide range of conditions including temperature, hydration and potential. The durability of polymer electrolyte membrane (PEM) fuel cell materials currently poses a major challenge to fuel cell commercialization for automotive applications [2].

Carbon-supported platinum is the most common catalyst for the oxygen reduction reaction (ORR) and is incorporated in the cathode catalyst layer (CCL) in a PEMFC. Not surprisingly, the performance of the fuel cell is strongly influenced by the CCL and particularly its compositional and morphological characteristics [3]. Major functions of the CCL are to reduce the activation barrier for the ORR, facilitate oxygen and water transport and conduct heat, protons and electrons. Consequently, degradation of the CCL has major impacts on the entire cell and system. The degradation of the cathode carbon catalyst supports in particular is one of the failure modes that can cause severe voltage degradation during operation. Thus, in order to further improve catalyst design, it is important to identify the key failure mechanisms of cathode degradation. A complication when assessing many automotive failure modes is that more than one mode of degradation of the catalyst layer usually operates at the same time, making it difficult to identify which one has the largest impact and thus is the most important failure mode to mitigate.

* Corresponding author. Tel.: +1 519 888 4567x33415; fax: +1 519 746 4979.
E-mail address: mfowler@uwaterloo.ca (M.W. Fowler).

0378-7753/$ – see front matter © 2013 Elsevier B.V. All rights reserved.
http://dx.doi.org/10.1016/j.jpowsour.2013.03.033

Carbon corrosion and Pt dissolution are two mechanisms by which the CCL commonly degrades [4]. Generally, carbon corrosion occurs as a result of carbon oxidation and the water–gas shift reaction [5]:

$$C + 2H_2O \rightarrow CO_2 + 4H^+ + 4e^- \qquad E_0 = 0.207\ V_{RHE}\ 25\ ^\circ C \tag{1}$$

Oxidation can also be driven by the heterogeneous reaction:

$$C + H_2O \rightarrow CO + 2H^+ + 2e^- \qquad E_0 = 0.518\ V_{RHE}\ 25\ ^\circ C \tag{2}$$

Carbon corrosion generally occurs under conditions in which the potential changes rapidly such as during continual cycling at high frequency or high oxidizing potentials are applied [6]. Carbon corrosion from the catalyst layer causes catalyst 'wash out' and/or aggregation of support and catalyst particles [7–10].

In order to study carbon corrosion, many bench scale in-situ accelerated stress tests (AST) have been developed [4]. These tests are usually aimed at identifying the specific life-limiting factors of the fuel cell materials and the degradation mechanisms on the basis of durability studies. Carbon corrosion can theoretically begin to occur at an electrode potential of 0.207 V_{RHE} [4] (where RHE denotes reversible hydrogen electrode). At cathode potentials above 0.8 V, a variety of carbon surface oxides have been observed to form [10,11]. In another study, carbon corrosion was found to accelerate when cathode potentials exceeded 1.2 V [4]. During normal PEMFC operation, the cathode potential is reported to vary between 0 and 1.0 V_{RHE}. However, under conditions of fuel starvation or gas switching such as during start-up and shutdown accelerated stress test protocols, the cathode potential is expected to exceed 1.2 V_{RHE} and lead to carbon oxidation. Hence, on the basis of these results, carbon corrosion can be observed by holding or switching the cathode potential above 1.2 V_{RHE}. This can be achieved by switching the voltage across the MEA (cell potential) between 1.0 and 1.4 V. The use of this potential window during accelerated stress tests is generally considered to be appropriate to assess carbon corrosion [12]. In this range, the role and mechanism of carbon corrosion, when the cathode catalyst is exposed to different upper potentials, are well known [10]. Holding the MEA at a constant cell voltage (usually between 1.0 and 1.4 V) is another approach to study carbon corrosion [6,11,13–15]. This approach requires a longer time to observe the degradation of the catalyst which is a disadvantage for screening and analyzing catalyst support materials. The rationale behind holding the PEMFC cell potential at 1.4 V to study carbon corrosion is that this is close to the PEM fuel cell cathode potential during the reverse current [16,17] and local fuel starvation [18] conditions, which lead to severe carbon corrosion [3]. Also, 1.4 V is the maximum potential at which oxygen evolution occurs only to a negligible extent. Once oxygen gas evolution is observed, then mechanical detachment of carbon black particles from the electrode can occur. The performance loss measured when the potential is held at 1.4 V is mainly due to carbon corrosion alone [6,8].

Pt loss during cell operation is another source of cathode layer degradation during durability experiments [4,5,19]. Pt loss during experiments has been estimated from the loss of Pt/C catalyst mass in acidic electrolyte systems after potential cycling [20,21]. Dissolution of Pt particles is generally caused by many factors such as Pt dissolution and wash out [5,20–22]. The occurrence of Pt dissolution has been reported under standard operating conditions [23]. Cycling the potential across the MEA over different potential ranges can cause severe voltage loss during the Pt degradation process, while higher potentials have been found to accelerate Pt dissolution and cause higher performance loss. Wang et al. [24] reported that the concentration of dissolved Pt increased monotonically as the cell potential is raised from 0.65 to 1.1 V, but then decreased at cell potentials higher than 1.1 V due to the formation of a protective oxide film. This trend is supported by another study that showed Pt dissolution to strongly increase with electrode potential in the region of 0.6–1.0 V versus RHE [25]. Therefore, the upper cell potential limit to assess Pt catalyst degradation is generally 1.0 V to avoid the possibility of carbon support corrosion. In addition, the agglomeration of Pt can also be affected by many other operating conditions such as temperature and/or relative humidity [26–29].

Platinum dissolution from the catalyst layer involves either direct dissolution by electrochemical oxidation or formation of oxide films by chemical reactions. Electrochemical dissolution of Pt to Pt^{2+} is described by the reactions below [4,24]:

$$Pt \rightarrow Pt^{2+} + 2e^- \qquad E_0 = 1.19 + 0.029 \log [Pt^{2+}] \tag{3}$$

The formation of PtO and its subsequent chemical reaction can occur as follows:

$$Pt + H_2O \rightarrow PtO + 2H^+ + 2e^- \qquad E_0 = 0.98 - 0.59\ pH \tag{4}$$

$$PtO + 2H^+ \rightarrow Pt^{2+} + H_2O \qquad \log [Pt^{2+}] = -7.06 - 2\ pH \tag{5}$$

The accelerated stress tests employed to study the simultaneous degradation of both the Pt catalyst and the carbon support generally operate at cell voltages between 0.6 V and 1.4 V. Such experiments under conditions where both modes of degradation occur together are important for several reasons. The presence of Pt has been found to catalyze CO_2 formation and carbon support corrosion at 0.8 V [8]. In contrast, in the absence of Pt, CO_2 tends to form only at potentials above 1.1 V [6,8,10,15]. However, the direct contribution of the Pt catalyst to carbon corrosion is not well understood. Furthermore, failure modes in automotive applications where both mechanisms operate are also of interest. Start-up/shut down (SU/SD) degradation generally involves situations where the cathode half-cell potential can reach voltages greater than 1.4 V [8] for short periods of time. During SU/SD cycles, both Pt dissolution and carbon corrosion likely contribute to the overall performance loss. In order to select the best mitigation strategy, it is necessary to identify the dominant mechanism that contributes to maximum performance loss. Currently, no method is available to do so.

One of the main objectives of this study is to identify diagnostic indicators or 'fingerprints' of performance degradation due to carbon loss using accelerated stress tests, which can provide direct information on carbon corrosion. The fingerprints are obtained by relating the amount of voltage loss to the amount of CO_2 that is generated during an accelerated stress test. The fingerprints are then used to deconvolute the performance losses due to carbon corrosion and Pt dissolution during a voltage cycle where degradation by both Pt dissolution and carbon corrosion occurs. The deconvoluted performance loss attributed to Pt dissolution is then compared to the performance loss during a voltage cycle, which targets only Pt dissolution, to validate the procedure. Finally, the limitations of the method when it is applied to different MEA types and when fuel cell performance is measured at different current densities will be discussed.

2. Experimental

2.1. Membrane electrode assemblies (MEAs) and structure

MEA testing was conducted using core automotive test (CAT) cell hardware designed by Automotive Fuel Cell Cooperation (AFCC). The active area of the test cell MEAs used in this study was 48.4 cm^2 [30]. The cathode catalyst used was TEC10EA50 catalyst from TKK. Three

different MEA types were made with this cathode catalyst type. MEA 1 and 2 are catalyst coated membrane-based MEAs, whereas the MEA 3 is a gas diffusion layer electrode-based MEA. All MEAs are perfluorosulfonic acid (PFSA) based re-enforced membranes. The experiments on fingerprint generation and performance loss de-convolution were primarily done using the 0.4 mg cm^{-2} loaded cathode which is denoted as MEA 1. The experiments on the MEAs with loading levels of 0.25 (denoted MEA 2) and 0.5 mg cm^{-2} (MEA 3) were used to assess the success of the de-convolution procedure with different MEA types. The anode and cathode gas diffusion layers (GDL) were made from common commercially available carbon fiber papers with a carbon and Teflon sub-layer or 'micro-porous layer' on both the electrodes.

2.2. Fuel cell operating conditions

The operating conditions for the different experiments conducted in this study are given in Table 1. The sequence of steps followed for each MEA subjected to an accelerated stress test protocol is as follows: i) conditioning, ii) electrochemical platinum surface area (EPSA) measurement, iii) measurement of a polarization curve, iv) accelerated stress test, v) cell recovery and vi) re-measurement of the polarization curve. The details involved in each experimental step are discussed below.

2.2.1. Conditioning

In all experimental studies, the fuel cells were conditioned for 12 h at a constant current density of 2.0 A cm^{-2}, 100% RH and 70 °C with the hydrogen and air flowrates maintained at 2 and 8 slpm, respectively. The flow rates of the reactant gases were maintained well above the stoichiometric levels to ensure that neither reactant became depleted within the fuel cell and that the hydrogen and oxygen concentrations would remain uniform and at known levels within the anode and cathode portions of the MEA, respectively. After conditioning, experiments to evaluate the beginning-of-life (BOL) performance were conducted.

2.2.2. Electrochemical platinum surface area measurement

After conditioning, the electrochemical platinum surface area was determined by CO-stripping voltammetry. Cyclic voltammograms were carried out using a load bank power supply to determine the electrochemical platinum surface area and the double-layer capacitance C_{dl} using methods similar to those that are generally accepted [31]. These experiments were conducted using H_2 as the feed gas stream to the anode at a flow rate of 2 slpm and 100% RH and N_2 containing 1% CO as the feed to the cathode at a flowrate of 12 slpm and 100% RH. The cathode potential was swept between 0.1 and 1.2 V at a scan rate of 20 mV s^{-1}. The double layer capacitance was measured at 0.45 V [32].

Table 1
Operating conditions during MEA experiments

	Conditioning	Polarization	EPSA	Accelerated stress tests	Recovery
Load (A cm^{-2})	2.0	0–2.4	0	0	0
Temperature (°C)	70	60	60	70	70
Fuel/oxidant gas	H_2/air	H_2/air	H_2/N_2	H_2/N_2	H_2/N_2
Fuel/oxidant pressure (barg)	1.7/1.5	1.7/1.5	1.5/1.5	1.5/1.5	0.4/0.03
Fuel/oxidant flowrate (slpm)	2/8	2/12	2/12	1/1	1/0
Fuel/oxidant relative humidity (%)	100/100	100/100	100/100	100/100	50/50

2.2.3. Polarization curve measurement

Following the electrochemical platinum surface area measurement, the cell performance was evaluated by determining the steady state polarization curve using H_2 and air as the fuel and oxidant at flow rates of 2 slpm and 12 slpm, respectively, and operating at 100% RH and 60 °C at both the anode and cathode. To obtain each point on the polarization curve, the steady state cell voltage was obtained at each applied current density over the range from 2.4 A cm^{-2} down to 0 A cm^{-2}.

2.2.4. Accelerated stress tests

Each of the MEAs was subjected to accelerated stress tests with the following cell voltage waveforms to measure the extent of carbon corrosion, mixed mode degradation and Pt dissolution: i) square wave voltage cycles between 1.0 V and 1.4 V with dwell times of 30 s and 30 s, respectively, ii) square wave voltage cycles between 1.0 V and 1.5 V with dwell times of 5 s and 5 s, respectively, iii) constant cell voltage of 1.4 V for durations varying from 5 h to 30 h between each measurement of fuel cell performance (i.e., measurement of polarization curve), iv) square wave voltage cycles between 0.6 V and 1.4 V with dwell times of 30 s and 30 s, respectively, and v) square wave voltage cycles between 0.6 V and 1.4 V with dwell times of 27 s and 3 s, respectively. The square wave voltage profile for each condition is given in Fig. 1.

The influence of the accelerated stress test on cell performance was evaluated by re-measuring the polarization curves after every 300 cycles until the end-of-life (EOL) point of 1500 total cycles was reached and after 5 h in the case when the cell voltage was held at a constant potential of 1.4 V. These polarization curves were obtained using the identical procedure to that described above.

2.2.5. Cell recovery

After completion of every 300 voltage cycles in all experiments, the cell was allowed to recover by flowing H_2 at 50% RH and 70 °C through the anode at a rate of 1 slpm for 4 h. No oxidant gas was passed through the cathode during this period.

2.2.6. CO_2 measurement

Throughout each accelerated stress test, the carbon dioxide content in the exhaust gas was measured using a Model 100 Infrared Analyzer (California Analytical Instruments). From this measurement, the amount of carbon lost due to corrosion was calculated.

3. Results and discussion

3.1. Carbon corrosion accelerated stress tests

To develop a fingerprint for the effect of carbon corrosion on performance loss, three accelerated stress tests are applied: constant cell potential of 1.4 V, a square wave cycle with 30 s at 1.0 V and 30 s at 1.4 V and a square wave cycle with 5 s at 1.0 V and 5 s at 1.5 V. The cell potential is elevated above 1.0 V during each of the accelerated stress tests to accelerate carbon corrosion and a cycle is applied in two cases. Lower voltage limits during the accelerated stress test cycles are maintained at 1.0 V to avoid platinum dissolution. The results obtained for MEA 1 are plotted in Fig. 2. Experiments at each condition were repeated three times and found to yield very reproducible results that differed less than 5%. Each of the performance loss values shown in Fig. 2 is the averages over these three separate measurements. The performance loss is obtained from the polarization curve by subtracting the cell voltage obtained for each MEA in its beginning-of-life condition at a given current from the voltage measured for the same MEA after the accelerated stress test at the same current. The performance losses

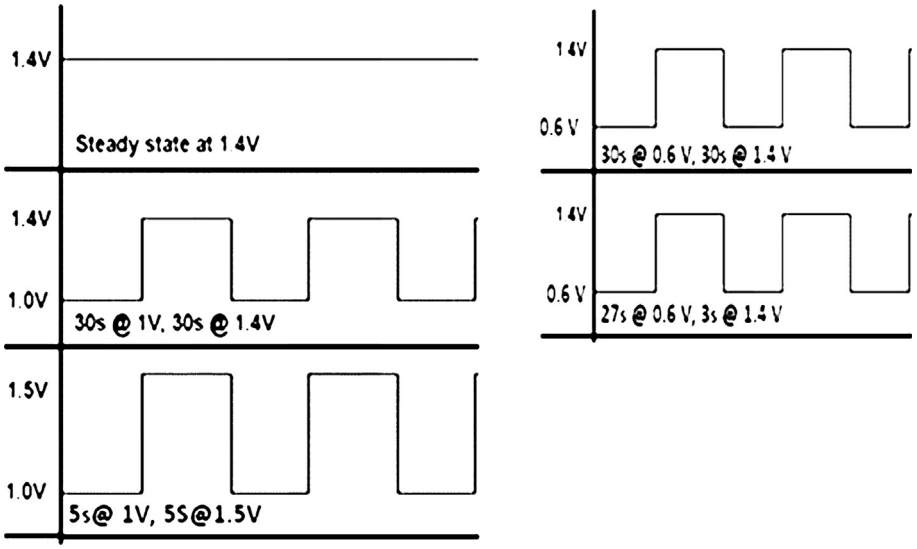

Fig. 1. Schematics of voltage cycles used to test the MEAs for carbon corrosion, mixed degradation and Pt dissolution. Operating conditions during accelerated stress tests are given in Table 1.

due to these three accelerated stress tests are found to be very similar over the first 20 h of operation. The application of the 1–1.4 V, 30 s–30 s voltage cycle accelerated stress test to MEA 1 leads to a potential decay of 200 mV at 1 A cm^{-2} by the end of 20 h of operation. A performance drop of 203 mV is observed after the accelerated stress test in which the voltage is held constant at 1.4 V for 20 h. The accelerated stress test comprised of 1.0–1.5 V, 30 s–30 s voltage cycles causes a 215 mV drop from its initial performance.

3.2. Fingerprint for carbon corrosion

It is evident from earlier studies that the degree of carbon corrosion and therefore the performance loss are affected by the nature of the accelerated stress test [10]. A fingerprint for carbon corrosion cannot be obtained by relating performance loss only to the number of cycles or hours of operation since the rate of corrosion also depends on other factors such as voltage and temperature. However, the observation of a similar magnitude of performance loss during each of the three accelerated stress tests supports the conclusion that carbon corrosion is the dominant mode of degradation in each case and that the impacts of carbon corrosion on cell performance can be similar although the exact testing conditions may differ.

The most direct measurement of carbon corrosion in an operating fuel cell is the amount of carbon dioxide produced which allows the total carbon loss to be calculated. In order to explore whether a correlation exists between the amount of carbon corrosion and the performance loss, the voltage loss over the course of the accelerated stress test is plotted against cumulative carbon loss. The performance loss measured at 1.0 A cm^{-2} for MEA 1 during the 1.4 V-hold accelerated stress test is shown in Fig. 3. These results show that even when the total carbon lost during this accelerated stress test reaches as high as 6 mg, which represents 30% of the initial amount present, this loss has very little effect on fuel cell performance. However, any further corrosion begins to have a dramatic effect and causes an exponential-like rise in performance loss. It is widely accepted that when a MEA is subjected to a constant potential at 1.4 V, the main driver for degradation is carbon corrosion. Based on the assumption that no other significant

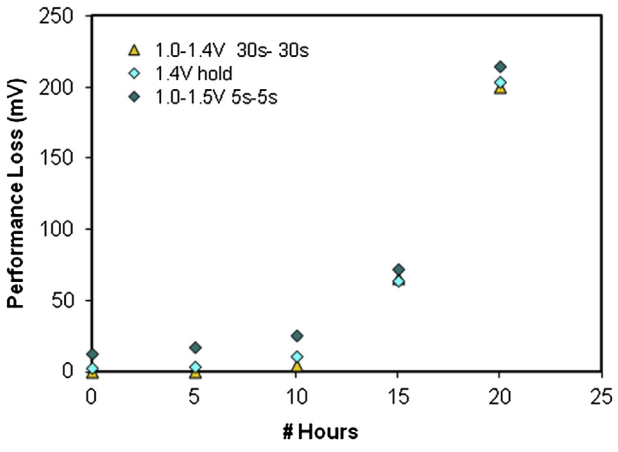

Fig. 2. Evolution of performance loss of MEA 1 with time during carbon corrosion accelerated stress tests. Performance loss is taken as the decrease in cell voltage from beginning-of-life value measured at a current density of 1 A cm^{-2} during polarization experiment. Operating conditions during accelerated stress tests and polarization experiments are given in Table 1.

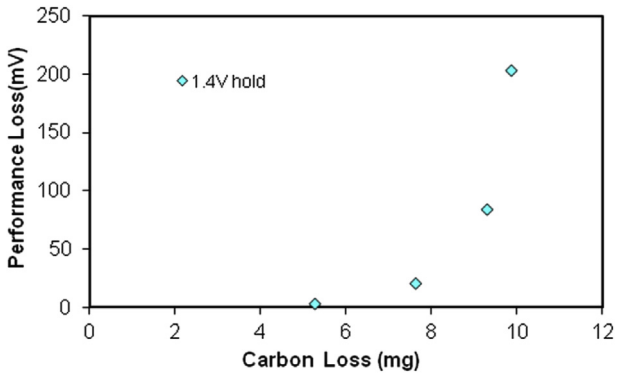

Fig. 3. Fingerprint relation between performance loss and cumulative carbon loss for MEA 1 obtained during accelerated stress test in which cell voltage is held at 1.4 V. Operating conditions during the accelerated stress tests and polarization experiments are given in Table 1.

degradation mechanism operates in this test, we consider Fig. 3 to define the performance loss due to carbon corrosion and refer to it as a carbon corrosion fingerprint for MEA 1.

3.3. Validation of carbon fingerprint with different carbon corrosion accelerated stress tests

To validate the carbon corrosion fingerprint shown in Fig. 3, performance and carbon loss data were obtained for MEA 1 using other accelerated stress tests, as discussed in Section 3.1. The performance losses of MEA 1 measured at 1.0 A cm^{-2} after being subjected to the three accelerated stress tests are plotted against carbon loss in Fig. 4a, while the corresponding losses obtained at 1.7 A cm^{-2} are presented in Fig. 4b. These results show that the fingerprints obtained using the two square-wave voltage cycles are virtually identical to the one measured during the 1.4 V-hold accelerated stress test at both current densities. A repeat experiment was conducted for each experimental condition and found to yield identical results to that shown for each accelerated stress test in Fig. 4. Despite having different upper potentials and cycles, the correlations of carbon loss data to performance loss are the same in all cases. This excellent agreement provides support that the accelerated stress test in which the potential is held at 1.4 V can be used to determine the amount of carbon corrosion. In order to use this data to deconvolute the performance loss when mixed modes of degradation are operating, an exponential function relating performance loss Y (in mV) to mass of carbon loss x (in mg) was fit to the data in Fig. 4a to yield what is termed the 'fingerprint equation' for carbon corrosion. The resulting empirical expression and correlation coefficient (R^2) obtained at 1.0 A cm^{-2} for MEA 1 when subjected to the three carbon corrosion accelerated stress tests is presented in Table 2.

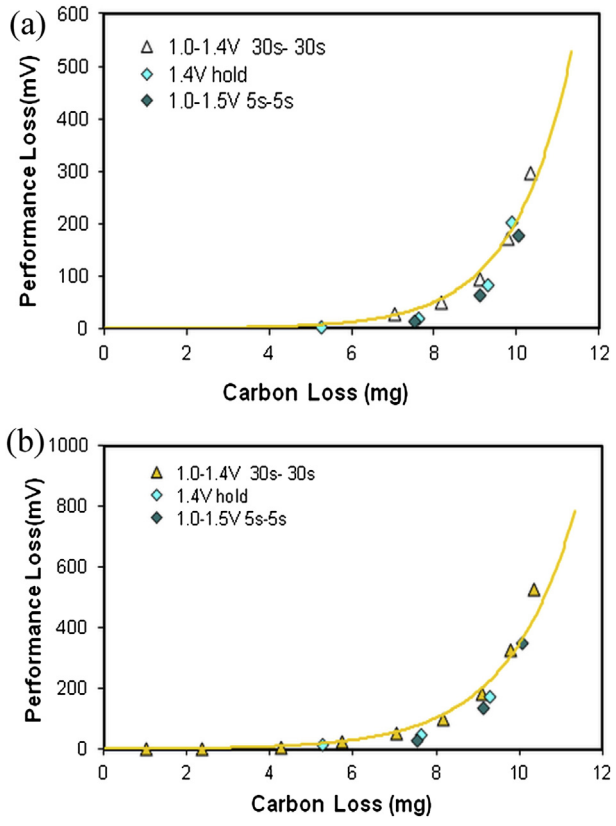

Fig. 4. Fingerprint relation between performance loss and cumulative carbon loss for MEA 1 obtained during carbon corrosion accelerated stress tests. Performance losses are measured at current densities of (a) 1 and (b) 1.7 A cm^{-2} during polarization experiment. Solid lines correspond to empirical fingerprint expressions fitted to experimental data. Operating conditions during the accelerated stress tests and polarization experiments are given in Table 1.

3.4. Pt dissolution and mixed degradation accelerated stress tests

An accelerated stress test in which platinum dissolution is believed to be the dominant degradation mode was also applied to MEA 1. This accelerated stress test consisted of a square wave cycle with lower and upper voltages of 0.6 and 1.4 V and dwell times of 27 s at the lower limit and 3 s at the upper limit. Pt dissolution should be the predominant mode of degradation during this accelerated stress test since the cell voltage is maintained at the lower voltage of 0.6 V for 90% of the time during each cycle. An upper limit of 1.4 V was used so that the results obtained from this accelerated stress test could be effectively compared with those obtained after the carbon corrosion accelerated stress tests. However, to minimize the amount of carbon corrosion, a short dwell time at the upper potential was selected to ensure that Pt dissolution is the primary mode of degradation [4,19]. The variation of the carbon loss with the number of square wave cycles obtained during the Pt dissolution accelerated stress test is compared to that measured during the 1.0–1.4 V, 30 s–30 s accelerated stress test in Fig. 5a. Not surprisingly, the carbon loss increases with the number of cycles during both accelerated stress tests. An essentially linear dependence is followed over the entire course of the 0.6–1.4 V, 27 s–3 s accelerated stress test. Comparison of the amount of carbon loss during this accelerated stress test to that obtained during the 1.0–1.4 V, 30 s–30 s accelerated stress test suggests that carbon corrosion should have minimal impact on the overall cell performance.

The mixed degradation accelerated stress test is a combination of the Pt dissolution accelerated stress test and the carbon corrosion accelerated stress test using square-wave cycles from 0.6 V to 1.4 V with 30 s dwell times at each potential to promote both Pt dissolution and carbon corrosion. The effect of the mixed degradation accelerated stress test on carbon loss is also included in Fig. 5a. As would be expected, the application of this accelerated stress test leads to greater carbon loss than the 1.0–1.4 V, 30 s–30 s accelerated stress test where carbon corrosion is predominant and the 0.6–1.4 V, 27 s–3 s accelerated stress test where Pt dissolution is predominant over the entire course of the cycling procedure. The carbon loss increases linearly over the earlier stages of the mixed degradation accelerated stress test, but begins to slow down after approximately 1000 cycles. Similar behavior is observed during the 1.0–1.4 V, 30 s–30 s accelerated stress test although the linear dependence persists as long as 2000 cycles.

Since degradation should occur primarily by Pt dissolution during the 0.6–1.4 V, 27 s–3 s accelerated stress test and by carbon

Table 2
Empirical equations relating performance loss Y measured at 1.0 A cm^{-2} to carbon mass loss x

	MEA	AST	Fingerprint equations[a]	R^2
Fig. 4a	MEA 1	1.0–1.5 V, 5 s–5 s 1.0–1.4 V, 30 s–30 s 1.4 V hold	$Y = 0.174e^{0.70x}$	0.98
Fig. 7a	MEA 1	1.0–1.5 V, 5 s–5 s	$Y = 0.025e^{13.695x}$	0.98
	MEA 2	1.0–1.5 V, 5 s–5 s	$Y = 0.605e^{16.69x}$	0.97
	MEA 3	1.0–1.5 V, 5 s–5 s	$Y = 0.211e^{6.16x}$	0.98

[a] In Fig. 4a, Y denotes performance loss measured in mV and x denotes carbon mass loss expressed in mg. In Fig. 7a, Y denotes % voltage loss and x denotes fraction of the initial carbon mass that is lost.

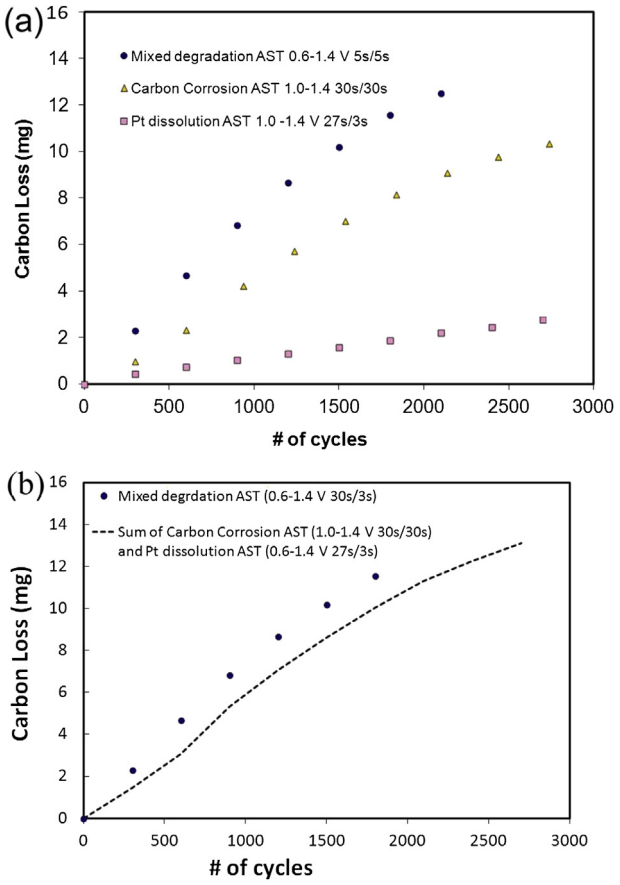

Fig. 5. (a) Variation of cumulative carbon loss in MEA 1 with number of cycles during carbon corrosion (1.0–1.4 V, 30 s–30 s), Pt dissolution (0.6–1.4 V, 27 s–3 s) and mixed degradation (0.6–1.4 V, 30 s–30 s) accelerated stress tests. (b) Comparison of carbon losses during mixed degradation test (symbols) to combined carbon losses during Pt dissolution and carbon corrosion tests (dotted line). Operating conditions during the accelerated stress tests and polarization experiments are given in Table 1.

corrosion during the 1.0–1.4V, 30 s–30 s accelerated stress test, it is interesting to compare the sum of the carbon losses during these accelerated stress test to the carbon losses measured during the mixed mode 0.6–1.4 V, 30 s–30 s cycles. As shown in Fig. 5b, this sum (dashed line) is found to lie below the carbon losses due to the 0.6–1.4 V, 30 s–30 s cycles. Nevertheless, it should be possible to determine the portion of the total performance loss due to Pt oxidation/dissolution by the application of an accelerated stress test such as 0.6–1.4V, 27 s–3 s square wave cycles and the portion due to carbon corrosion by application of an accelerated stress test such as 1.0–1.4 V, 30 s–30 s cycles. The carbon losses during the accelerated stress test expected to be dominated by carbon corrosion (1.0–1.4 V, 30 s–30 s cycles) and mixed mode degradation (0.6–1.4 V, 30 s–30 s cycles) are as much as 4 and 5 times, respectively, larger than that associated with Pt dissolution alone. This observation supports the use of the carbon corrosion fingerprint equation directly to deconvolute the effect of Pt dissolution from the total performance loss for any mixed degradation accelerated stress tests.

3.5. Deconvolution technique

In this section, a method to deconvolute the contributions to the performance loss arising from a mixed degradation voltage cycle accelerated stress test (0.6–1.4 V, 30 s–30 s square wave cycle) is presented for MEA 1. The resulting breakdown of the performance losses at 1.0 and 1.7 A cm^{-2} are shown in Fig. 6a and b, respectively. The method is summarized as follows. First, the carbon loss from the MEA is estimated from the amount of carbon dioxide present in the exhaust gas at each sampling point during the mixed degradation accelerated stress test. It is interesting that exponential functions are also found to fit the performance loss–carbon loss data very well at both current densities after this accelerated stress test (solid black curves in Fig. 6a and b). Next, the performance loss due to carbon corrosion is calculated using the carbon fingerprint equation described in Sections 3.2 and 3.3. The calculated performance loss due to carbon corrosion is then subtracted from the total mixed degradation performance loss to yield the carbon corrosion-corrected performance loss, which is attributed to Pt dissolution. Finally, this carbon corrosion-corrected performance loss is compared to the loss measured after the Pt dissolution accelerated stress test (0.6–1.4 V, 27 s–3 s square wave cycle).

Comparison of the experimental data after the 0.6–1.4 V, 27 s–3 s and 0.6–1.4 V, 30 s–30 s accelerated stress tests indicates that Pt oxidation/dissolution accounts for almost all the performance loss at 1.0 A cm^{-2} until the completion of approximately 600 accelerated stress test cycles (Fig. 6a). Beyond this stage, the overall

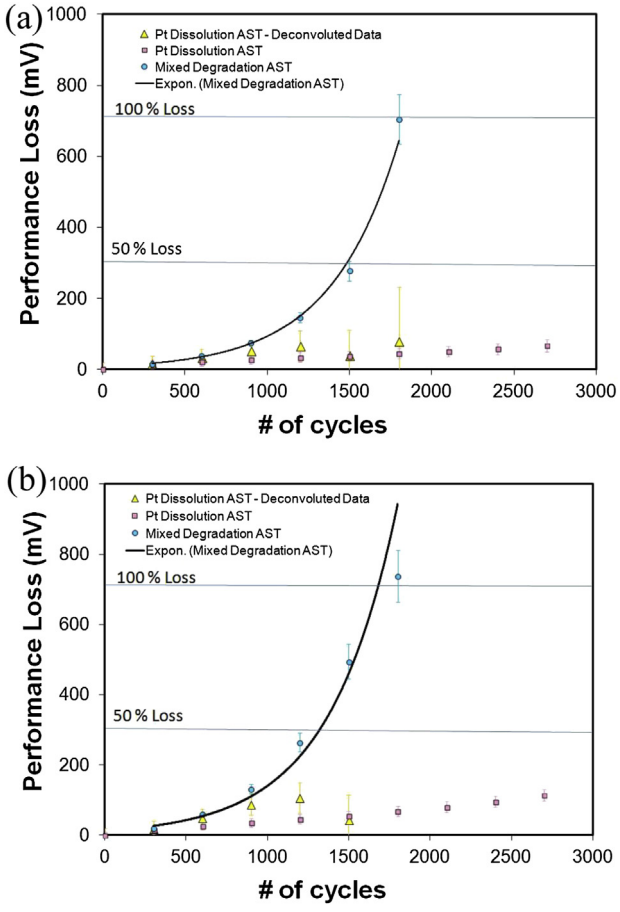

Fig. 6. Comparison of variation of performance loss of MEA 1 with number of cycles measured during Pt dissolution accelerated stress test (pink symbols) to that obtained using deconvolution method (solid yellow curve). Performance losses are measured at current densities of (a) 1 and (b) 1.7 A cm^{-2} during polarization experiment. Also included is corresponding behavior during mixed degradation test obtained from measurements (blue symbols) and empirical expressions (solid black curve) fitted to experimental data. Horizontal blue lines correspond to points where performance losses of 50 and 100% are reached (For interpretation of the references to color in this figure legend, the reader is referred to the web version of this article.).

performance loss begins to rise much more sharply, whereas the Pt dissolution-induced performance loss continues to increase only very slightly. This indicates that carbon corrosion does not become significant immediately after the start of the 0.6–1.4 V, 30 s–30 s accelerated stress test and only begins to become dominant after about 600 cycles under these conditions. The curves (solid yellow lines) obtained from the difference between the performance losses after the 0.6–1.4 V, 30 s–30 s and 1.0–1.4 V, 30 s–30 s accelerated stress test at both current densities are in good agreement with those measured after the 0.6–1.4 V, 27 s–3 s accelerated stress test until approximately 1500 cycles have been applied and the performance loss is close to 50% (For interpretation of the references to color in this paragraph, the reader is referred to the web version of this article.).

In order to assess the reliability of this approach to de-convolute the effects due to both degradation modes, we conducted similar analysis of performance loss at several other current densities between 0.5 and 1.7 A cm^{-2}. The results obtained at 1.7 A cm^{-2} are shown in Fig. 6b as an example. At all of these current densities, very similar behavior to that at 1.0 A cm^{-2} is observed. Pt oxidation/dissolution contributes to virtually all of the performance loss up to about 500–600 cycles. Again, the error in inferring the contribution of Pt oxidation/dissolution from the difference in the performance losses during the 0.6–1.4 V, 30 s–30 s and 1.0–1.4 V, 30 s–30 s accelerated stress tests becomes large beyond about 1500 cycles. Thus, a performance loss of about 50% appears to be the upper limit at which the contribution of Pt oxidation/dissolution can be accurately determined on the basis of data obtained from only the 0.6–1.4 V, 30 s–30 s and 1.0–1.4 V, 30 s–30 s accelerated stress test without also applying the 0.6–1.4 V, 27 s–3 s accelerated stress test. However, it should be noted that most of the accelerated drive cycle tests used to evaluate PEM fuel cell performance do not usually continue beyond 50% performance loss in the MEA. In this case, the error in estimating the contribution of Pt oxidation/dissolution from the difference in the performance losses after 0.6–1.4 V, 30 s–30 s and 1.0–1.4 V, 30 s–30 s accelerated stress tests alone may be acceptable.

A factor that may contribute to the error in estimating the contribution of Pt oxidation/dissolution in the later stages of these experiments is that the performance losses measured during the 0.6–1.4 V, 30 s–30 s and 1.0–1.4 V, 30 s–30 s accelerated stress tests both become large. Since the difference between two large quantities is being used to estimate the much smaller performance loss due to Pt oxidation/dissolution, a significant error in this estimation can arise from the inevitable experimental errors associated with the measurement of the performance losses during the 0.6–1.4 V, 30 s–30 s and 1.0–1.4 V, 30 s–30 s accelerated stress tests. In this situation, it is preferable to determine the contribution of Pt oxidation/dissolution directly from an accelerated stress test such as 0.6–1.4V, 27 s–3 s square wave cycles.

3.6. Limitations of deconvolution method

Repeat experiments with each of the carbon corrosion accelerated stress tests for MEA 1 showed good reproducibility in generating the empirical correlations. In order to further assess the value of the fingerprint equations generated, it is important to evaluate their ability to predict the performance loss of other types of MEAs. Consequently, fingerprint curves and expressions for carbon corrosion in MEA 2 and MEA 3 were generated. As with MEA 1, the measurements obtained on these MEAs were found to be very reproducible. Also, very similar trends were observed with these MEAs.

To compare the performance losses obtained in the three MEAs, the loss of voltage in each MEA is normalized with respect to its beginning-of-life cell voltage since the degradation of a MEA is affected by its initial state. Thus, the following equation is used:

$$\%\ \text{Performance loss} = \frac{V_{\text{BOL}} - V_{n-\text{th cycle}}}{V_{\text{BOL}}} \times 100 \quad (6)$$

where V_{BOL} is the cell voltage of the beginning-of-life sample and $V_{n-\text{th cycle}}$ is the voltage after the n-th cycle. In addition, the carbon losses in a MEA are expressed as percentages of the initial mass present to account for the differences in the amount initially present in the various MEAs. Fig. 7a presents plots of the percentage performance loss of each MEA versus the percentage carbon loss up to its end-of-life state obtained from direct experimental measurements at 1.0 A cm^{-2}. The corresponding results obtained at 1.7 A cm^{-2} are shown in Fig. 7b. In all cases, accelerated stress tests which favor carbon corrosion were applied in order to obtain the fingerprint relations. Also included are the data obtained for MEA 1 after application of the 1.0–1.4 V, 30 s–30 s and the constant 1.4 V accelerated stress tests. The 1.0–1.5 V, 5 s–5 s accelerated stress tests were repeated for each MEA to assess the reproducibility of the protocols used. The results from these experiments are also included in Fig. 7 and show excellent reproducibility in all cases.

Although the plots in Fig. 7 for the three MEAs are similar to each other in shape and follow exponential behavior, they do not

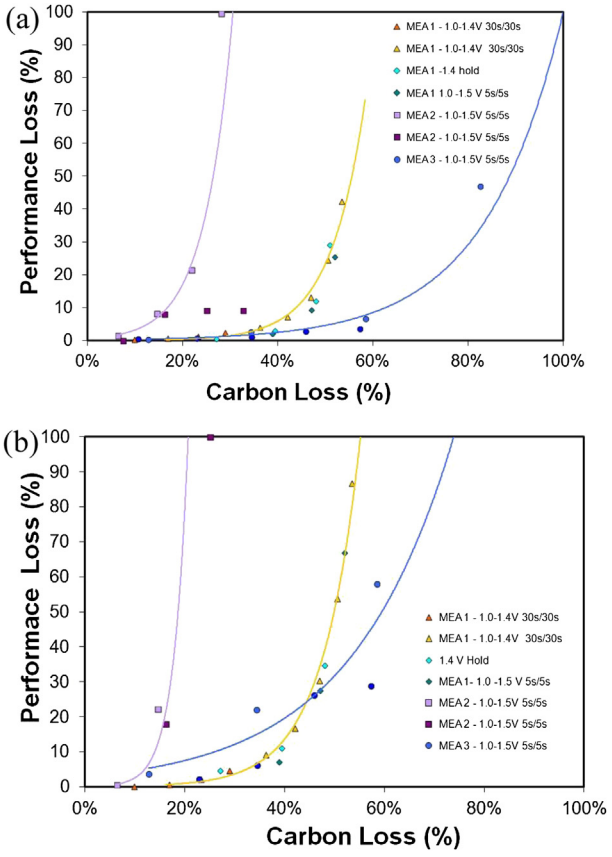

Fig. 7. Fingerprint relations between percent performance loss and percent carbon loss for MEA 1, MEA 2 and MEA 3 obtained during carbon corrosion accelerated stress tests. (a) Performance losses are measured at current densities of (a) 1 and (b) 1.7 A cm^{-2} during polarization experiment. Measurements are denoted by symbols, while solid lines (yellow – MEA 1, purple – MEA 2, blue – MEA 3) show behavior corresponding to empirical fingerprint expressions fitted to experimental data. Operating conditions during the accelerated stress tests and polarization experiments are given in Table 1 (For interpretation of the references to color in this figure legend, the reader is referred to the web version of this article.).

fall along a single universal curve. The behavior for each MEA follows a separate curve, revealing that a separate fingerprint equation is required in each case. Plots of the exponential expressions fitted to the experimental data relating % performance loss to % carbon mass loss in MEA 1 and MEA 2 during the 1.0–1.5 V, 5 s–5 s accelerated stress tests are included as the solid curves in Fig. 7a and b. The parameters for these expressions are also listed in Table 2. As with MEA 1, exponential functions are found to fit the experimental data very well for MEA 2 and MEA 3. The fact that the behavior of each MEA follows a separate curve indicates that the performance loss due to carbon corrosion depends on other factors such as the loading level of cathode Pt/C catalyst and the structure and chemistry of the membrane and GDL. Nevertheless, the results shown in this study hold promise that the approach proposed here of developing fingerprint expressions relating performance loss to carbon loss and deconvoluting the contributions from different degradation modes through combined analysis of specifically chosen accelerated stress tests can be extended to a wide variety of MEAs.

4. Conclusions

A MEA with 0.4 mg Pt cm^{-2} loading (MEA 1) has been tested with various accelerated stress test protocols in a CAT cell. Performance indicators of carbon corrosion or performance 'fingerprints' have been identified using several carbon corrosion accelerated stress tests. Each fingerprint takes the form of an empirical exponential expression correlating the performance loss to the carbon loss during these accelerated stress test cycles. It provides an excellent fit between carbon loss and performance loss provided it is restricted to a given MEA and should prove useful as a tool to predict performance loss in drive cycle tests of full-size fuel cells.

This fingerprint also forms a critical component of a newly proposed deconvolution method to estimate the performance loss contributions due to Pt oxidation/dissolution and carbon oxidation during mixed degradation tests. This approach has been has been shown to successfully estimate the contributions of these two degradation modes measured at various current densities between 0.5 and 1.7 A cm^{-2}. The deconvolution method appears to be a robust technique for the analysis of performance loss after carbon corrosion and mixed degradation accelerated stress tests. Only two accelerated stress tests, namely those for which carbon corrosion and mixed degradation are dominant, are required to accurately determine the contribution of Pt oxidation/dissolution as long as the performance loss does not reach above approximately 50%. Above 50% performance loss (a region of less interest for the modeling of overall fuel cell system degradation), the contribution of Pt oxidation/dissolution can be best determined by application of an accelerated stress test in which this mechanism is dominant. More work is required to extend this approach to different MEAs and different operating conditions such as relative humidity and temperature. In addition, other possible degradation mechanisms beyond Pt oxidation/dissolution and carbon corrosion that operate at large current densities and when % carbon loss becomes high should be identified.

Identification of carbon corrosion indicators and a deconvolution procedure for separation of Pt loss and carbon corrosion represents an important step for studying the durability of fuel cells for automotive applications. Implementation of the empirical models for carbon corrosion into fuel cell research should prove useful for predicting MEA lifetimes. At a more fundamental level, approach adopted in this study of combining the use of specifically chosen accelerated stress test procedures should aid in future investigations on the relation between performance loss and different catalyst degradation modes.

Acknowledgments

The authors are grateful to the Natural Sciences and Engineering Research Council of Canada (NSERC) for funding support to carry out this research. They also acknowledge the NSERC Industrial Postgraduate Scholarship (NSERC – IPS) program for providing a scholarship for one of the authors (SRD).

References

[1] S.R. Dhanushkodi, M.W. Fowler, A.G. Mazza, M.D. Pritzker, Membrane electrode assembly contamination, in: H. Li, Z. Shi, J.W. Van Zee (Eds.), Proton Exchange Membrane Fuel Cells: Contamination and Mitigation Strategies, CRC Press, 2010, p. 151.
[2] M.W. Fowler, R.F. Mann, J.C. Amphlett, B.A. Peppley, P.R. Roberge, J New Mater. Electrochem. Syst. (2002) 255–262.
[3] Y. Shao, G. Yin, Y. Gao, J. Power Sources 171 (2007) 558–566.
[4] R. Borup, J. Meyers, B. Pivovar, Y.S. Kim, R. Mukundan, N. Garland, D. Meyers, M. Wilson, F. Garzon, D. Wood, P. Zelenay, K. More, K. Stroh, T. Zawodzinski, J. Boncella, J.E. McGrath, M. Inaba, K. Miyatake, M. Hori, K. Ota, Z. Ogumi, S. Miyata, A. Nishikata, Z. Siroma, Y. Uchimoto, K. Yasuda, K.-i. Kimijima, N. Iwashita, Chem. Rev. 107 (2007) 3904–3951.
[5] F.A.d. Bruijn, V.A.T. Dam, G.J.M. Janssen, Fuel Cells 8 (2008) 3–22.
[6] Y. Shao, J. Wang, R. Kou, M. Engelhard, J. Liu, Y. Wang, Y. Lin, Electrochim. Acta 54 (2009) 3109–3114.
[7] W.R. Baumgartner, E. Wallnofer, T. Schaffer, J.O. Besenhard, V. Hacker, V. Peinecke, P. Prenninger, ECS Trans. 3 (2006) 811–825.
[8] N. Linse, L. Gubler, G.G. Scherer, A. Wokaun, Electrochim. Acta 56 (2011) 7541–7549.
[9] L.M. Roen, C.H. Paik, T.D. Jarvi, Electrochem. Solid-State Lett. 7 (2004) A19–A22.
[10] S. Maass, F. Finsterwalder, G. Frank, R. Hartmann, C. Merten, J. Power Sources 176 (2008) 444–451.
[11] K.H. Kangasniemi, D.A. Condit, T.D. Jarvi, J. Electrochem. Soc. 151 (2004) E125–E132.
[12] H. Schulenburg, B. Schwanitz, N. Linse, G.n.G. Scherer, A. Wokaun, J. Krbanjevic, R. Grothausmann, I. Manke, J. Phys. Chem. 115 (2011) 14236–14243.
[13] H. Zhong, H. Zhang, G. Liu, Y. Liang, J. Hu, B. Yi, Electrochem. Commun. 8 (2006) 707–712.
[14] M.F. Mathias, R. Makharia, H.A. Gasteiger, J.J. Conley, T.J. Fuller, C.J. Gittleman, S.S. Kocha, D.P. Miller, C.K. Mittelsteadt, T. Xie, S.G. Van, P.T. Yu, Electrochem. Soc. Interface 14 (2005) 24–35.
[15] S. Ball, S. Hudson, B. Theobald, D. Thompsett, ECS Meeting, 2007, MA 2007-02 (9) (2007) 396.
[16] S.D. Knights, K.M. Colbow, J. St-Pierre, D.P. Wilkinson, J. Power Sources 127 (2004) 127–134.
[17] C.A. Reiser, L. Bregoli, T.W. Patterson, J.S. Yi, J.D. Yang, M.L. Perry, T.D. Jarvi, Electrochem. Solid-State Lett. 8 (2005) A273–A276.
[18] T.W. Patterson, R.M. Darling, Electrochem. Solid-State Lett. 9 (2006) A183–A185.
[19] J. Wu, X.Z. Yuan, J.J. Martin, H. Wang, J. Zhang, J. Shen, S. Wu, W. Merida, J. Power Sources 184 (2008) 104–119.
[20] S.C. Ball, S.L. Hudson, J.H. Leung, A.E. Russell, D. Thompsett, B.R.C. Theobald, J. Power Sources 171 (2007) 18–25.
[21] S. Mitsushima, S. Kawahara, K.-i. Ota, N. Kamiya, J. Electrochem. Soc. 154 (2007) B153–B158.
[22] Z. Luo, D. Li, H. Tang, M. Pan, R. Ruan, Int. J. Hydrogen Energy 31 (2006) 1831–1837.
[23] S. Zhang, X.-Z. Yuan, J.N.C. Hin, H. Wang, K.A. Friedrich, M. Schulze, J. Power Sources 194 (2009) 588–600.
[24] X. Wang, R. Kumar, D.J. Myers, Electrochem. Solid-State Lett. 9 (2006) A225–A227.
[25] J. Aragane, T. Murahashi, T. Odaka, J. Electrochem. Soc. 135 (1988) 844–850.
[26] M. Cai, M.S. Ruthkosky, B. Merzougui, S. Swathirajan, M.P. Balogh, S.H. Oh, J. Power Sources 160 (2006) 977–986.
[27] T. Yoda, H. Uchida, M. Watanabe, Electrochim. Acta 52 (2007) 5997–6005.
[28] R.L. Borup, J.R. Davey, F.H. Garzon, D.L. Wood, M.A. Inbody, J. Power Sources 163 (2006) 76–81.
[29] H. Xu, R. Kunz, J.M. Fenton, Electrochem. Solid-State Lett. 10 (2007) B1–B5.
[30] E. Hillstrom, Design and validation of a subscale PEMFC test hardware, in: Proceedings Hydrogen + Fuel cells International Conference, Vancouver, Canada, May 15–18, 2011.
[31] J. Wu, X.Z. Yuan, H. Wang, M. Blanco, J.J. Martin, J. Zhang, Int. J. Hydrogen Energy 33 (2008) 1735–1746.
[32] K.-S. Lee, B.-S. Lee, S.J. Yoo, S.-K. Kim, S.J. Hwang, H.-J. Kim, E. Cho, D. Henkensmeier, J.W. Yun, S.W. Nam, T.-H. Lim, J.H. Jang, Int. J. Hydrogen Energy 37 (2012) 5891–5900.